

Facial Demorphing from a Single Morph Using a Latent Conditional GAN

Nitish Shukla and Arun Ross
 Michigan State University
 {shuklan3, rossarun}@msu.edu

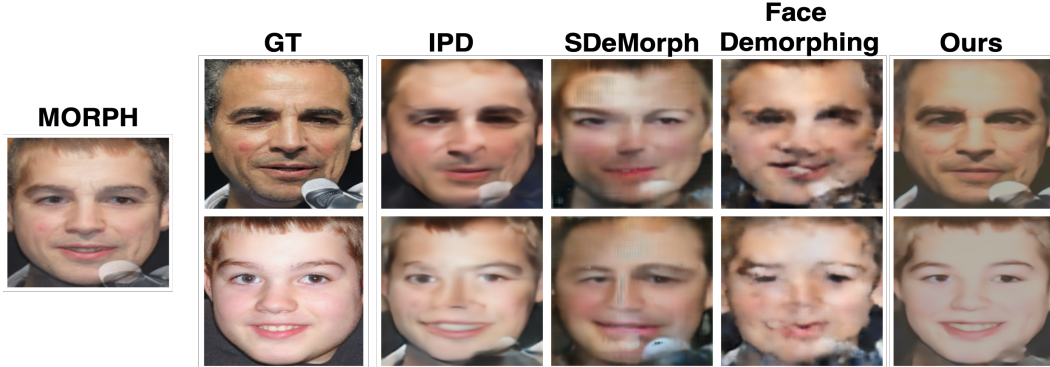


Figure 1. Comparison with current state-of-the-art demorphing methods under a unified training protocol: Our method surpasses current methods, viz., Identity-Preserving Demorphing (IPD) [54], SDeMorph [52] and Face Demorphing [7], in terms of both visual quality and analytical performance. Notably, i) the outputs from our method look dissimilar from each other, and ii) outputs faithfully match the corresponding ground truth both in the pixel and latent spaces.

Abstract

A morph is created by combining two (or more) face images from two (or more) identities to create a composite image that is highly similar to all constituent identities, allowing the forged morph to be biometrically associated with more than one individual. Morph Attack Detection (MAD) can be used to detect a morph, but does not reveal the constituent images. Demorphing - the process of deducing the constituent images - is thus vital to provide additional evidence about a morph. Existing demorphing methods suffer from the morph replication problem, where the outputs tend to look very similar to the morph itself, or assume that train and test morphs are generated using the same morph technique. The proposed method overcomes these issues. The method decomposes a morph in latent space allowing it to demorph images created from unseen morph techniques and face styles. We train our method on morphs created from synthetic faces and test on morphs created from real faces using different morph techniques. Our method outperforms existing methods by a considerable margin and produces high fidelity demorphed face images.

1. Introduction

How can we efficiently recover the constituent images from a single face morph image? A face morph is created by mixing two (possibly more) face images belonging to different individuals while ensuring that it biometrically matches with all participating identities [42, 50]. Morphs can evade manual detection [21, 36], enabling multiple individuals to gain access using a single document [36, 38], making them an obvious security threat [57]. Deducing constituent face images from a single morph - known as demorphing - has been a crucial yet challenging task. Demorphing is an ill-posed inverse problem, where the challenge lies not only in the absence of the knowledge of the morphing technique used (landmark-based or deep learning based) but also in the lack of constraints on the output space. In this paper, we propose a new framework to separate constituent face images from a single morph image. Our method operates under a more realistic evaluation (see Section 2) and achieves high facial fidelity in demorphing images (see Figure 1).

Demorphing, just like morph attack detection (MAD), can be either i) reference-based [19, 39, 20, 9, 33, 8], i.e., an image of one of the constituent identities is available besides the morph image, or ii) reference-free [52, 7, 54], i.e., no additional information is available besides the morph image. Single image reference-free demorphing is a sig-

nificantly challenging task compared to its reference-based counterpart. Indeed, given a single morph image, with no additional constraints in output image space, there can be an infinite number of possible decomposed pairs. Moreover, developing a unified framework to demorph images created using different morphing techniques is equally challenging. Our method learns to produce the most likely set of face images conditioned on the input morph.

Demorphing in Latent Space: Learning the process of demorphing can be divided into two stages: perceptual compression, which discards unimportant details while preserving semantics, followed by generative modeling of the decomposition process in the latent space. Operating in latent space simplifies learning by offering a perceptually equivalent but more tractable domain [44]. To achieve this, we first learn an autoencoder that projects the input image into a lower dimensional but perceptually equivalent and computationally efficient latent space, and second, we train a conditional GAN [35], conditioned on the input morph image to effectively separate it into its constituent images in this latent space.

In addition to being computationally efficient, a key advantage of our method is that, unlike prior approaches, the demorpher needs to be trained only once. This is because it operates directly on latent representations, which are already disentangled from image-level noise and artifacts. The compression stage captures only the important semantic features, ignoring the unimportant attributes in the pixel space (background, morphing artifacts, etc.). This means that our method can handle morphs made using unseen morphing techniques and faces despite never being trained on them. We refer to our method as *Latent Conditional GAN*.

Another key challenge is the limited availability of datasets for demorphing, and privacy issues related to the use or sharing of real face data. Existing morph datasets are mainly designed for morph attack detection and typically contain only around 1.5K morphs, which is insufficient for training generative models. To address these limitations, we train our method on morphs created using synthetically generated face images, thereby simultaneously addressing both privacy and data scarcity.

In summary, our contributions are as follows:

- In contrast to previous work [7, 54, 52], our method has fewer constraints and operates under a realistic protocol.
- Unlike previous methods, our method is agnostic to morphing technique and face style (passport style, background, etc). Our method can be used for general demorphing (see Section 8).
- We experimentally show that by demorphing in latent space, our method not only overcomes *morph replication*, where a model tends to reproduce the morph

image as its outputs, it also suppresses high-frequency artifacts in recovered images.

2. Background

Morphing typically combines two face images of two distinct individuals. Traditionally, morphing has been accomplished by geometrically aligning facial landmarks and superimposing the second image on top of the *base image* [40, 14]. Due to this formulation, morphs typically are biased toward one of the participating images, leaving very little visual information about the second image for faithful recovery. Recently, deep morphing methods have been proposed [10, 59, 48, 28] that create morphs from the ground up, making demorphing even more challenging. A morphing operator, \mathcal{M} , acts on two face images, i_1 and i_2 , to produce the morph x , i.e., $x = \mathcal{M}(i_1, i_2)$. The goal of the morphing operator is to create a morph such that i) the morph looks reasonable in terms of perceptual image quality in pixel space, and ii) the morph matches both i_1 and i_2 with respect to a biometric matcher \mathcal{B} , i.e., $\mathcal{B}(x, i_n) > \tau$, $n \in \{1, 2\}$ and τ is the matching threshold depending on the application scenario. Reference-free demorphing attempts to approximate the inverse of the morphing process. Given a morphed input, x , the goal is to recover the images used to create the morph. Reference-free demorphing is an ill-posed inverse problem [7, 52].

A demorphing operator, $\mathcal{DM} (= \mathcal{M}^{-1})$, upon receiving the morph image, x , attempts to reconstruct the original constituent images, $o_1, o_2 = \mathcal{DM}(x)$, satisfying the conditions:

$$\mathcal{B}(o_1, o_2) < \theta \quad (1)$$

$$\min_{j \in \{1, 2\}} \max_{\substack{k \in \{1, 2\} \\ k \neq j}} \{ \mathcal{B}(o_j, i_k), \mathcal{B}(o_k, i_j) \} > \epsilon \quad (2)$$

where, θ and ϵ are matching thresholds. Eq. (1) enforces the reconstructed outputs to appear dissimilar to each other and Eq. (2) ensures that each reconstructed output aligns with its corresponding ground truth image.

In the literature, demorphing has been explored under different scenarios based on how the training and testing morphs are composed [54, 53]. Consider a set \mathcal{Y} of face images used to create morphs (train and test). The scenarios below are illustrated in Figure 3.

1. **Same identities in training and testing:** Both train and test morphs are created from face images in \mathcal{Y} . However, the same *pair* of identities are not used to generate both train and test morphs.
2. **Partially unseen identities:** Here, the face set \mathcal{Y} is divided into two disjoint sets with disjoint identities, \mathcal{Y}_1 and \mathcal{Y}_2 . The train morphs are exclusively created from identities in \mathcal{Y}_1 whereas test morphs are created using one identity in \mathcal{Y}_1 and another in \mathcal{Y}_2 .

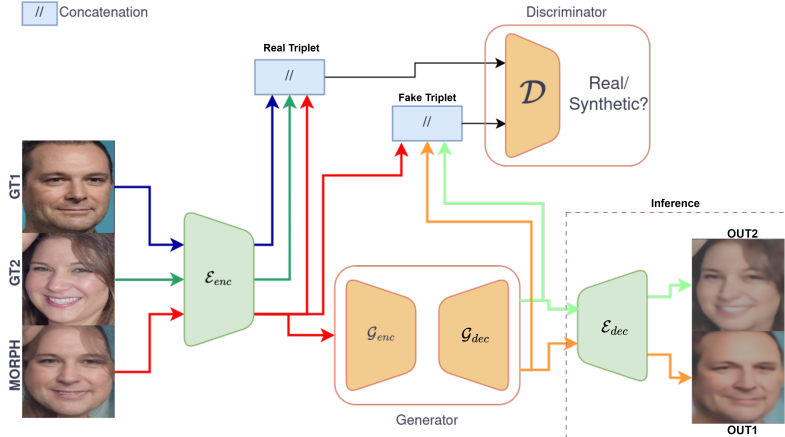


Figure 2. Proposed Demorphing Architecture: An encoder, \mathcal{E}_{enc} , compresses the morph along with the constituent face images during training. The generator, \mathcal{G} , reconstructs two face images conditioned on the morph in \mathcal{E}_{enc} 's latent domain. The discriminator distinguishes between real and synthesized face feature triplets. During inference, a decompressor, \mathcal{E}_{dec} , recovers the constituent images. Note that the decoder, \mathcal{E}_{dec} , is used only during inference to decompress the demorphed outputs.

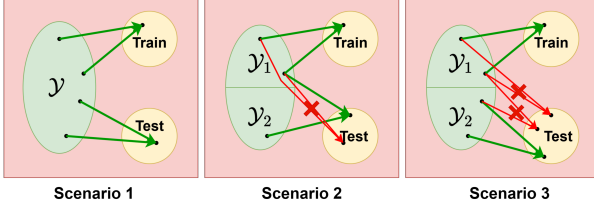


Figure 3. Scenarios in demorphing: Green arrows indicate a valid test morphs whereas red arrows indicate invalid test morphs in each scenario. (Left) Training and testing morphs are created with identities in \mathcal{Y} . (Middle) Test morphs are created using one identity in \mathcal{Y}_1 and another in \mathcal{Y}_2 . (Right) Train and test morphs are created using disjoint identities in \mathcal{Y}_1 and \mathcal{Y}_2 , respectively.

3. Completely disjoint identities: The identities used to create train morphs are completely disjoint from identities used to create the test morphs. In other words, the train morphs are exclusively created from identities in \mathcal{Y}_1 whereas test morphs are created exclusively from identities in \mathcal{Y}_2 .

In this paper, every identity in all of the datasets is represented by a single image. Train morphs are generated using synthetic face images, while test morphs are created exclusively from neutral face images in the FRL face dataset. Consequently, the terms “images” and “identities” are sometimes used interchangeably.

3. Previous Work

In [7], the authors propose a GAN-based approach to demorphing inspired by [62]. Their method includes a generator and three discriminators. Although the original technique effectively separated natural scene images, it faced a challenge known as morph-replication when applied to

demorphing, where the model tended to generate two outputs that closely resembled the morph. This problem arises because of the high degree of local similarity within face images compared to scene images. Moreover, the method assumes that the train and test morphs are created using the same morph technique. Shukla [52] introduced a demorphing approach using diffusion models [23], which iteratively adds noise to the morphed image and retrieves the constituent faces during the reverse process. However, this approach assumes that both train and test morphs are derived from the same set of face images, i.e., scenario 1. In [54], the authors propose decomposing the morphed image into multiple unintelligible, privacy-preserving components and then reconstructing the constituent images by weighing and merging these components. This method also presumes shared identities in the train and test morphs. While these techniques achieve varying levels of success, they are generally too restrictive for practical real-world applications.

In [43], authors propose a reference-based demorphing technique based on diffusion autoencoders. Their method employs pretrained diffusion autoencoders to encode the image into two subspaces: a semantic latent space that captures identity features and a stochastic latent space that retains the remaining stochastic details. The accomplice's face image is restored by decoding the latent code of two subspaces via a conditional denoising diffusion implicit model. FD-GAN [39] is another reference-based method that employs a dual architecture, aiming to reconstruct the first identity's image from the morphed input using the second identity's image as a reference. To assess the generative model's effectiveness, it subsequently attempts to recover the second identity using the reconstructed image of the first identity as input.

In this work, we propose a reference-free demorph-

ing technique free of two critical assumptions, i) morph-technique used to create test morphs and ii) the bonafide identities in train and test morphs.

4. Methodology

We pose the training of our method as a pixel-wise regression problem in latent space guided by an adversarial loss function and kurtosis regularization. Our method consists of an image compressor, \mathcal{E} , a demorphing generator, \mathcal{G} , and a discriminator, \mathcal{D} . Figure 2 shows an overview of our method. Our method first perceptually compresses the input morph using the encoder, \mathcal{E} . This step effectively eliminates unimportant high-level visual features that are not critical for demorphing. Another advantage of compressing the input image is the standardization of the representation, i.e., face images are represented in the encoder’s latent domain eliminating distractors like background, morph artifacts, lighting, etc. The backbone of our method is based on a conditional-GAN. An image-to-image generator, \mathcal{G} , conditioned on the encoded morph images, demorphs the morph in the latent space. A discriminator concatenates the encoded morph with the encoded demorphed outputs and the corresponding ground truth images, and distinguishes between real and synthetic triplets. We optimize the GAN within the latent space of \mathcal{E} , which offers two key advantages. (i) Computational efficiency: Since the weights of \mathcal{E} remain frozen, high-resolution face images are represented using lower-dimensional tensors, significantly accelerating both the training and inference processes. (ii) Perceptual Loss: Computing losses in latent space eliminates the need to compare irrelevant features. For instance, the same face image with different backgrounds may exhibit a significantly higher per-pixel loss in the RGB domain, whereas the difference is much smaller in the latent space. During inference, the decoder, \mathcal{E}_{dec} , decodes the demorphed outputs produced by the generator.

4.1. Face Image Compression

Our face compression model is based on [32], consisting of an autoencoder trained with KL Loss ensuring that the reconstructions are confined to the image manifold by enforcing local realism and preventing the blurriness often caused by relying exclusively on pixel-space losses like L_2 or L_1 . Specifically, given an image $x \in \mathbb{R}^{H \times W \times 3}$ in RGB space, the encoder, \mathcal{E}_{enc} , compresses the image into a latent representation $z = \mathcal{E}_{enc}(x) \in \mathbb{R}^{h \times w \times c}$. Symmetrically, a decompressor, \mathcal{E}_{dec} , reconstructs the image \tilde{x} from the latent representation such that $\tilde{x} = \mathcal{E}_{dec}(z) = \mathcal{E}_{dec}(\mathcal{E}_{enc}(x))$. The compressor downscales the height and width of the image image by a factor 2^3 each such that $h = H/8$ and $w = W/8$. In practice, we use a pretrained autoencoder employed in Stable Diffusion [45] trained on KL Loss. For an image of size $512 \times 512 \times 3$, the autoencoder produces a

latent of size $64 \times 64 \times 4$. The weights of the autoencoder remain frozen during the entire training process.

4.2. Demorphing

We train our demorpher to reduce the distance between the generated demorphed outputs and ground truths in latent space. Unlike prior approaches [7, 52, 54], we explicitly order the outputs but randomly swap the ground-truth pairs during training. This allows us to train with varied pair orderings using a standard per-pixel loss (see Figure 6), enabling a more robust generation across both reconstructed images by exposing the model to both possible orders.

Latent conditional GAN: With our trained compressing network, \mathcal{E} , we now perform demorphing in an efficient low-dimensional latent space abstracting away the unnecessary imperceptible details in the RGB pixel space. Performing demorphing in latent space not only makes the process computationally efficient, but also makes it more suitable for the method to focus on important semantic bits of data. The backbone of our method is a conditional GAN [25]. The generator, \mathcal{G} , and discriminator, \mathcal{D} , are conditioned on the morph, x . Consider a morph, x , created using two face images, i_1 and i_2 , then the conditional GAN loss can be stated as:

$$\begin{aligned} \mathcal{L}_{cGAN}(\mathcal{G}, \mathcal{D}) = & \mathbb{E}_{x,i}[\log \mathcal{D}(x, i)] \\ & + \mathbb{E}_{x,z}[\log(1 - \mathcal{D}(x, \mathcal{G}(x, z)))] \end{aligned} \quad (3)$$

where, $i = (i_1, i_2)$ represents the outputs. To enforce consistency between the generated and real outputs, we also incorporate an \mathcal{L}_1 loss:

$$\mathcal{L}_1 = \mathbb{E}_{x,i,z}[||i - \mathcal{G}(x, z)||_1]. \quad (4)$$

Morph Replication: In [7], authors use a GAN to demorph face images which is based on [62]. Despite having a separation critic, their method suffered from *morph-replication*, where the model tends to output the morph itself as both of its outputs. This is primarily due to the intrinsic local similarities in face images compared to natural scene images. Indeed, comparing two passport-style face images (typically used in border control, driver’s license, etc.) in pixel space would lead to their average being the pairwise distance minimizer and still resembling a face. To alleviate this problem, we introduce another constraint on the prior. We introduce a kurtosis loss that minimizes the difference in kurtosis between the predicted outputs, $o = (o_1, o_2)$, and the ground truth, $i = (i_1, i_2)$:

$$\mathcal{L}_{kurt} = \sum_{j=1}^2 \left| \text{Kurt}(o_j) - \text{Kurt}(i_j) \right| \quad (5)$$

By aligning the higher-order statistics of the generated and real images, the kurtosis loss helps maintain the structural consistency and realism of the synthesized outputs.

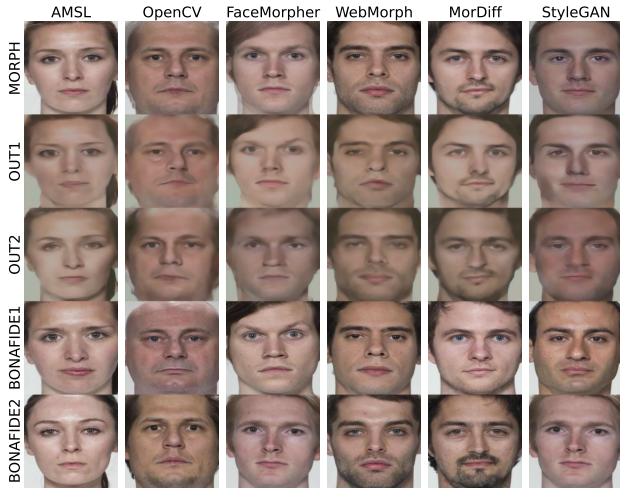


Figure 4. Reference-free demorphing: We test our method on the FRLL-Morph and MorDiff datasets. The model outputs OUT1 and OUT2 in arbitrary order on input MORPH. Our method produces visually distinct outputs i) between OUT1 and OUT2 and ii) between MORPH-OUT1 and MORPH-OUT2.



Figure 5. Our method ensures that both outputs maintain the same identity (since input only contains a single identity) when provided with a non-morphed input.

This loss is complementary to traditional losses, such as \mathcal{L}_1 and perceptual loss, which primarily focus on pixel-wise or feature-wise differences, but may overlook distributional properties. The final objective function incorporates the kurtosis loss alongside adversarial and reconstruction losses:

$$\mathcal{L} = \mathcal{L}_{\text{cGAN}} + \lambda_1 \mathcal{L}_1 + \lambda_2 \mathcal{L}_{\text{kurt}}, \quad (6)$$

where, λ_1 and λ_2 are set to 0.5 each. The inclusion of kurtosis loss enhances the perceptual quality of the generated images by ensuring that the outputs maintain similar statistical characteristics to the real data.

4.3. Implementation Details

We use the pretrained autoencoder employed by Stable Diffusion [45] trained on KL Loss. The autoencoder consists of four ResNet based downsampling and

upsampling blocks each with GroupNorm [58], dropout and the SiLU [17] activation function. Our generator, \mathcal{G} , is based on HuggingFace’s conditional UNet implementation, UNet2DConditionModel, comprising six ResNet-based downsampling blocks and six corresponding upsampling blocks. Self-attention mechanisms are included in the fifth downsampling block and the second upsampling block. The UNet also requires a timestep input, which we fix to zero in all experiments to neutralize its effect. The discriminator, \mathcal{D} , is based on CNN architecture composed of four sequential blocks, each containing a convolutional layer, Instance Normalization [56], and a LeakyReLU activation.

We evaluate our demorphing method using AdaFace [29] and ArcFace [16] face recognition models. We use cosine similarity to compute the biometric match score. Training is carried out using Adam optimization [31] with multi-GPU support via accelerate [22]. The training parameters are as follows: number of epochs: 300, learning rate: 10^{-4} , dropout rate: 0.1, β_1 : 0.5 and β_2 : 0.999.

5. Dataset

Test datasets: We test our proposed method on three well-known morph datasets: AML [37], FRLL-Morphs [15], and MorDiff [10]. The FRLL-Morphs dataset includes morphs generated using four different techniques: OpenCV [47], StyleGAN [28], WebMorph [14], and FaceMorph [40]. In all three datasets, the source (i.e., non-morph) images come from the FRLL dataset, which includes 102 identities, each represented by two frontal images — one smiling and one neutral — resulting in a total of 204 face images. The morph counts in each of the datasets are as follows: AML: 2,175 morphs; FaceMorph: 1,222 morphs; StyleGAN: 1,222 morphs; OpenCV: 1,221 morphs; WebMorph: 1,221 morphs; MorDiff: 1,000 morphs. The selection of test datasets includes both conventional landmark-based morph techniques and more recently introduced generative methods.

Train dataset: It is widely recognized that generative models require a large amount of training data to capture data distribution accurately. In the context of facial demorphing, a sufficiently large morph dataset is crucial for effective disentanglement. Additionally, the legal and ethical challenges of using/reusing/sharing real biometric data pose a significant challenge. Publicly available datasets are therefore inadequate for training a generalized demorphing technique due to: (i) their limited size (typically around 1.5k morphs) [11, 12, 18, 19, 41, 49] and (ii) privacy/legal issues [5, 6, 1, 3, 2, 4]. To train a high resolution demorphing generative method, we follow the training protocol proposed in [55]. To generate a morph, we sample two synthetic face images from SMDD train-set which is generated using StyleGAN2-ADA [26] trained on Flickr-Faces-

Table 1. Comparison of our method with the existing state-of-the-art demorphing techniques under a unified protocol. Our method outperforms IPD [54], SDeMorph [52] and Face Demorphing [7]. We assess our method using established image decomposition IQA metrics (PSNR/SSIM), demorphing metrics (Restoration Accuracy), and biometrically-weighted IQA (BW) [55]. The numbers included for the other methods have been computed by us.

Method	Metric	ArcFace						AdaFace					
		AMSL	OpenCV	FMorph	Wmorph	MorDiff	StyleGAN	AMSL	OpenCV	FMorph	Wmorph	MorDiff	StyleGAN
Ours	Rest. Acc. @ 10%FMR	99.90%	99.83%	100.00%	100.00%	38.76%	98.58%	99.53%	99.71%	100.00%	100.00%	50.39%	
	Rest. Acc. @ 1%FMR	99.09%	99.30%	99.03%	99.47%	100.00%	12.57%	96.35%	98.58%	98.57%	98.91%	100.00%	20.75%
	Rest. Acc. @ 0.1%FMR	96.26%	95.83%	95.16%	96.28%	98.63%	2.12%	91.19%	93.69%	93.41%	94.53%	98.83%	4.52%
	BW (SSIM)	0.44	0.49	0.49	0.46	0.50	0.32	0.35	0.38	0.38	0.36	0.41	0.12
	BW (PSNR)	10.12	11.56	11.56	10.56	11.07	7.30	7.92	9.02	9.09	8.22	9.05	2.79
IPD (2024) [54]	Restoration Accuracy	25.69%	40.54%	37.82%	25.61%	38.12%	16.22%	0.18%	1.89%	1.43%	0.31%	3.88%	0.00%
	BW (SSIM)	0.26	0.32	0.32	0.25	0.33	0.22	0.17	0.21	0.21	0.16	0.22	0.08
	BW (PSNR)	6.28	7.98	9.95	6.16	8.12	5.31	4.14	5.30	5.29	4.10	5.53	1.93
SDeMorph (2023) [52]	Restoration Accuracy	12.56%	15.62%	13.18%	12.80%	11.67%	0.00%	0.00%	0.00%	0.00%	0.00%	0.00%	0.00%
	BW (SSIM)	0.16	0.19	0.19	0.18	0.17	0.15	0.11	0.12	0.12	0.11	0.11	0.05
	BW (PSNR)	4.24	4.88	4.97	4.68	4.29	3.85	2.76	3.20	3.22	3.16	2.98	1.29
Face Demorphing (2022) [7]	Restoration Accuracy	0.45%	0.53%	0.51%	0.50%	0.62%	0.43%	0.17%	0.23%	0.17%	0.20%	0.29%	0.00%
	BW (SSIM)	0.21	0.24	0.25	0.23	0.29	0.19	0.11	0.14	0.13	0.13	0.16	0.06
	BW (PSNR)	4.46	5.21	5.50	4.93	6.13	4.13	2.39	2.95	2.89	2.82	3.33	1.31

Table 2. Comparison of demorphing quality using standard image quality assessment metrics: PSNR / SSIM. Higher values indicate better image reconstruction fidelity.

Method	AMSL	OpenCV	FaceMorpher	WebMorph	MorDiff	StyleGAN
Ours	10.81 / 0.47	11.65 / 0.50	11.63 / 0.49	11.17 / 0.49	10.93 / 0.49	10.18 / 0.45
IPD (2024) [54]	9.32 / 0.38	10.37 / 0.42	10.27 / 0.41	9.63 / 0.39	9.91 / 0.40	9.08 / 0.37
SDeMorph (2023) [52]	8.99 / 0.34	9.54 / 0.37	9.60 / 0.37	9.45 / 0.37	8.97 / 0.34	8.74 / 0.34
Face Demorphing (2022) [7]	9.68 / 0.46	10.35 / 0.48	10.44 / 0.47	10.20 / 0.48	10.13 / 0.47	9.51 / 0.45

HQ Dataset (FFHQ) dataset [27]. Choosing random images helps train more generalizable morph attack detection (MAD) systems [13]. We create morphed images using the widely adopted [12, 46, 51] OpenCV/dlib morphing algorithm [34], employing Dlib’slandmark detector implementation [30]. This landmark-based morphing approach generates morph attacks that are more effective than those produced by other tools [46]. With this strategy, we generate 15,000 train and test morphs (from 25K face images in SMDD train and test dataset) each. All images (train and test) are processed using MTCNN [60] to detect faces, after which the face regions are cropped. The images are then normalized and resized to a resolution of 512×512 . Images where faces cannot be detected are discarded. Notably, no further spatial transformations are applied, ensuring that the facial features (such as lips and nose) in both the morphs and the ground-truth constituent images stay aligned throughout training.

Identity Leakage: Although training with synthetic morphs offers advantages, it is essential to ensure that test identities are not inadvertently replicated during synthetic face generation. In other words, the identities used to create the training morph set should be distinct from those used for generating test morphs. This separation prevents identity leakage and ensures a fair evaluation of the model’s generalization capabilities. We assess identity leakage across 25,000 training face images, each representing a unique identity, and 204 (from 102 identities) test face images from the FRL dataset. This evaluation is conducted using two

face matchers, namely, ArcFace and AdaFace. We observe an average top $n\%$ (0.1,1,5) similarity of 0.22, 0.17, 0.13 between the two sets using the ArcFace matcher and 0.21, 0.16, 0.12 using AdaFace. These relatively low scores suggest that the identities in the test set are unlikely to be present in the training face set, indicating minimal identity leakage.

6. Evaluation

6.1. Existing Metrics

Reference-free face demorphing is a relatively recent development made possible by advancements in generative learning. There are three main evaluation metrics in the literature to benchmark demorphing methods, namely, True Match Rate at various False Match Rate thresholds, Restoration Accuracy (RA), and standard Image Quality Assessment metrics such as SSIM and PNSR. In [55], authors argue that TMR@FMR and RA focus only on biometric identity (and not image quality) whereas SSIM/PSNR focus only on quality (and not on biometric utility). Therefore, a comprehensive metric is needed to effectively capture the identities in the face matcher’s embedding domain as well as structural quality in pixel-space. This metric, proposed in [55], is described in the next sub-section.

6.2. Biometrically cross-weighted IQA

Let \mathcal{X} be the face morph set and \mathcal{Y} be the face images used to generate the morphs in \mathcal{X} and $\mathcal{M} : \mathcal{Y} \times \mathcal{Y} \rightarrow \mathcal{X}$ be the morphing operator. A demorpher $\mathcal{DM} : \mathcal{X} \rightarrow \mathcal{Y} \times \mathcal{Y}$ approximates \mathcal{M}^{-1} such that $\mathcal{DM}(x) = (o_1, o_2)$, which may not exist analytically. The goal of \mathcal{DM} is to ensure that *morph replication* does not occur, i.e., $o_1 \neq o_2 \neq x$. In other words, the outputs produced by \mathcal{DM} should look dissimilar (to the extent they really are), and the outputs should match the ground truth face images with respect to a biometric matcher \mathcal{B} . The biometrically weighted IQA [55]

Table 3. Effects of Separation Priors: We analyze the impact of different separation priors applied during training and find that the combination of kurtosis loss with the standard per-pixel loss yields the best performance among all tested approaches.

Metric	Dataset	$\ell_1 + \text{kurt}$	$\ell_1 \text{ only}$	$\ell_1 + \text{zhang}$	$\ell_1 + \text{cross}$	$\ell_1 + \text{triplet}$	$\ell_1 \text{ image}$	trivial
PSNR	AMSL	10.81	10.75	10.98	9.78	11.2	10.0	-
	OpenCV	11.65	11.48	11.67	10.21	11.83	10.78	-
	FaceMorpher	11.63	11.58	11.71	10.25	11.99	10.69	-
	WebMorph	11.17	11.07	11.4	10.12	11.45	10.43	-
	MorDiff	10.93	11.03	11.33	9.7	11.4	10.16	-
	StyleGAN	10.18	10.14	10.37	9.55	10.41	9.53	-
SSIM	AMSL	0.47	0.47	0.48	0.39	0.49	0.47	1.0
	OpenCV	0.5	0.49	0.5	0.40	0.51	0.49	1.0
	FaceMorpher	0.49	0.49	0.5	0.39	0.51	0.48	1.0
	WebMorph	0.49	0.49	0.5	0.41	0.51	0.48	1.0
	MorDiff	0.49	0.49	0.5	0.39	0.51	0.48	1.0
	StyleGAN	0.45	0.44	0.46	0.38	0.47	0.45	1.0
Restoration Accuracy	AMSL	99.89/98.57	70.04/53.60	71.77/59.20	32.72/27.02	98.55/97.93	99.61/99.33	99.11/99.71
	OpenCV	99.82/99.52	70.55/58.51	64.44/54.10	36.02/29.17	99.45/99.05	99.81/99.38	97.48/97.48
	FaceMorpher	100/99.71	77.10/55.30	67.16/54.72	32.36/27.50	99.65/98.85	100/99.77	98.28/98.28
	WebMorph	100/100	72.06/60.16	73.87/68.12	38.94/34.68	99.46/99.06	100/99.84	97.5/97.5
	MorDiff	100/100	89.74/80.54	87.71/85.99	55.98/34.68	99.55/99.77	100/100	100.00/100.00
	StyleGAN	38.56/50.39	9.12/9.98	5.14/6.55	0.50/0.15	42.93/48.67	61.15/67.70	97.5/97.5
BW(PSNR)	AMSL	7.92/10.12	7.62/10.16	3.30/4.82	2.69/6.80	7.34/9.86	6.86/8.40	-
	OpenCV	9.02/11.56	8.55/10.98	3.41/5.14	2.84/7.07	7.99/10.23	7.53/9.26	-
	FaceMorpher	9.09/11.56	8.72/10.86	3.43/5.38	2.85/7.26	7.89/10.43	7.30/9.38	-
	WebMorph	8.22/10.56	7.88/10.36	3.71/5.08	2.86/7.07	7.55/9.81	6.80/8.42	-
	MorDiff	9.05/11.07	8.66/10.80	4.6/6.4	3.07/6.82	8.57/10.37	6.82/8.58	-
	StyleGAN	2.79/7.3	2.66/6.99	1.3/3.8	1.36/5.62	2.77/7.09	2.29/5.83	-
BW(SSIM)	AMSL	0.35/0.44	0.33/0.44	0.15/0.21	0.11/0.27	0.32/0.43	0.32/0.40	-
	OpenCV	0.38/0.49	0.36/0.47	0.15/0.22	0.11/0.27	0.34/0.44	0.34/0.42	-
	FaceMorpher	0.38/0.49	0.37/0.46	0.15/0.23	0.11/0.27	0.33/0.44	0.33/0.42	-
	WebMorph	0.36/0.46	0.34/0.45	0.16/0.22	0.11/0.28	0.33/0.43	0.31/0.39	-
	MorDiff	0.41/0.5	0.39/0.48	0.20/0.28	0.12/0.27	0.38/0.46	0.32/0.40	-
	StyleGAN	0.12/0.32	0.12/0.30	0.06/0.17	0.05/0.22	0.12/0.31	0.11/0.27	-



Figure 6. A comparison of the results based on different image separation priors: Zhang’s exclusion loss [61], cross-road loss [62] and triplet loss [24].

is defined as

$$BW(iqa) = \mathbb{E}_{x \in \mathcal{X}} \max \left(\sum_{i \in \{1,2\}} \mathcal{B}(o_i, i_i) \cdot iqa(o_i, i_i), \sum_{\substack{i \in \{1,2\} \\ j=i \% 2 + 1}} \mathcal{B}(o_i, i_j) \cdot iqa(o_i, i_j) \right)$$

where, $\%$ is the modulo operator and $iqa \in \{SSIM, PSNR\}$. $BW(iqa)$ computes IQA between

two possible combinations of output-ground truth pairs and weighs them with the biometric match score produced by a face matcher.

7. Results

7.1. Comparison with State-of-the-Art Methods

Limited work exists in single-image reference-free demorphing. We compare our methods to three existing meth-

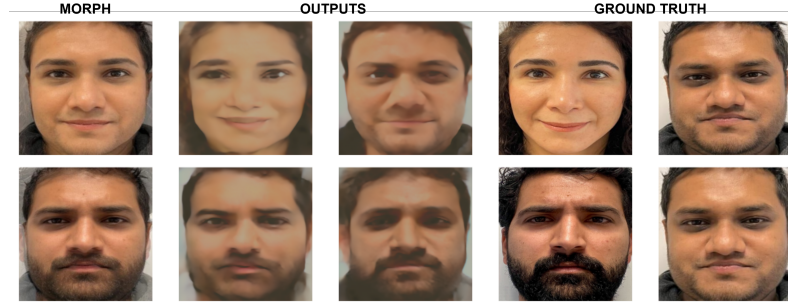


Figure 7. Testing on live subjects: Our method effectively separates the ground truth identities based on gender and facial features. All subjects agreed for publication.

ods. Table 1 and Table 2 show the quantitative comparison of our method against [52, 54]. We compare our method using existing metrics (TMR, Restoration Accuracy, IQA) as well as BW-IQA. Our method significantly outperforms existing methods in the proposed protocol across all metrics and datasets. Visually, our method is able to capture accurate facial features compared to previous methods (see Figure 1 and Figure 4). We also compare our method with [7]. On the AMSL dataset, our approach achieves a TMR of 97.77% using ArcFace, significantly outperforming their result of 70.55%.

7.2. Ablation Study

To evaluate the importance of demorphing in the latent space, we perform the same experiment in the RGB domain, i.e., \mathcal{E} is substituted with an identity function that outputs the input image as it is, keeping other settings unchanged. Table 3 shows the evaluation results of the two models and Figure 6 shows visual comparisons. Our method in the latent space clearly separates two faces and produces high-resolution images compared to blurry and less distinctive faces when demorphing is done in the pixel space.

8. Human Study

To assess the effectiveness of our approach, we perform demorphing on morphs generated from live samples. We gather 17 face images from various subjects (5 males, 3 females), instructing them to pose as if for a driver’s license photo, allowing them to decide on wearing or removing accessories such as jewelry or glasses. We created 28 morph images using the protocol described in Section 5, making sure that each pair of identities has at least one morph. We present few samples in Figure 7. Our method generates distinct outputs while preserving a high degree of similarity to the ground truth images. We observe a restoration accuracy of 95.65% with AdaFace and 91.30% with ArcFace. We also observe a PSNR of 10.66 and a SSIM value of 0.52. Finally, we evaluate the results using the BW(*iqa*) metrics. We observe a BW(SSIM) of 0.16 and 0.24 on AdaFace and

ArcFace, respectively, and a BW(PSNR) of 3.31 and 5.03. These results show the efficacy of the proposed method.

9. Conclusion

In this paper, we introduced a novel reference-free face demorphing framework, Latent Conditional GAN, which operates in a perceptually equivalent latent space to efficiently separate constituent faces from a single morph image. Unlike prior approaches, our method is agnostic to the morphing technique, scales to high-resolution images, and generalizes to unseen morph styles without retraining. By leveraging a latent-space representation, we not only mitigate the morph replication problem but also suppress unnecessary artifacts, ensuring higher facial fidelity in the recovered images. Our method surpasses existing methods by a considerable margin both in terms of analytical performance and visual fidelity. Future work will involve processing morphs generated using more than two images.

10. Acknowledgment

This project was funded by the NSF Center for Identification Technology (Award #1841517) and DHS CINA (Award #17STCIN00001-07-01).

References

- [1] The European Parliament and the Council of the European Union. Article 6(4)(c) of the general data protection regulation. 2016. 5
- [2] The European Parliament and the Council of the European Union. Article 9(2)(a) of the general data protection regulation. 2016. 5
- [3] The European Parliament and the Council of the European Union. Article 37(1) of the general data protection regulation. 2016. 5
- [4] The European Parliament and the Council of the European Union. Article 6(1)(a) of the general data protection regulation. 2016. 5
- [5] The European Parliament and the Council of the European Union. Article 9 of the general data protection regulation . 2016. 5

[6] The European Parliament and the Council of the European Union. Regulation (EU) 2016/679 of the european parliament and of the council of 27 April 2016 on the protection of natural persons with regard to the processing of personal data and on the free movement of such data, and repealing directive 95/46/ec (General Data Protection Regulation). 2016. 5

[7] Sudipta Banerjee, Prateek Jaiswal, and Arun Ross. Facial De-morphing: Extracting Component Faces from a Single Morph. In *Proceedings of IEEE International Joint Conference on Biometrics*, 2022. 1, 2, 3, 4, 6, 8

[8] Sudipta Banerjee and Arun Ross. Conditional identity disentanglement for differential face morph detection. In *Proceedings of IEEE International Joint Conference on Biometrics (IJCBI)*, pages 1–8, 2021. 1

[9] Juan Cai, Qiangqiang Duan, Min Long, Le-Bing Zhang, and Xiangling Ding. Feature Interaction-Based Face Demorphing Factor Prediction for Restoring Accomplice’s Facial Image. *Sensors*, 24(17), 2024. 1

[10] Naser Damer, Meiling Fang, Patrick Siebke, Jan Niklas Kolf, Marco Huber, and Fadi Boutros. MorDiff: Recognition Vulnerability and Attack Detectability of Face Morphing Attacks Created by Diffusion Autoencoders. In *Proceedings of 11th International Workshop on Biometrics and Forensics (IWBF)*, pages 1–6, 2023. 2, 5

[11] Naser Damer, Jonas Henry Grebe, Steffen Zienert, Florian Kirchbuchner, and Arjan Kuijper. On the generalization of detecting face morphing attacks as anomalies: Novelty vs. outlier detection. In *Proceedings of IEEE 10th International Conference on Biometrics Theory, Applications and Systems (BTAS)*, pages 1–5, 2019. 5

[12] Naser Damer, Alexandra Moseguí Saladié, Andreas Braun, and Arjan Kuijper. MorGAN: Recognition Vulnerability and Attack Detectability of Face Morphing Attacks Created by Generative Adversarial Network. In *Proceedings of 2018 IEEE 9th International Conference on Biometrics Theory, Applications and Systems (BTAS)*, pages 1–10, 2018. 5, 6

[13] Naser Damer, Alexandra Moseguí Saladié, Steffen Zienert, Yaza Wainakh, Philipp Terhörst, Florian Kirchbuchner, and Arjan Kuijper. To detect or not to detect: The right faces to morph. In *Proceedings of International Conference on Biometrics (ICB)*, pages 1–8, 2019. 6

[14] Lisa DeBruine. debruine/webmorph morphing software: Beta release 2, Jan. 2018. 2, 5

[15] Lisa DeBruine and Benedict Jones. Face Research Lab London (FRL) Image Dataset. May 2017. 5

[16] Jiankang Deng, Jia Guo, Niannan Xue, and Stefanos Zafeiriou. Arcface: Additive Angular Margin Loss for Deep Face Recognition. In *Proceedings of the IEEE/CVF Conference on Computer Vision and Pattern Recognition*, pages 4690–4699, 2019. 5

[17] Stefan Elfwing, Eiji Uchibe, and Kenji Doya. Sigmoid-weighted linear units for neural network function approximation in reinforcement learning. 2017. 5

[18] Matteo Ferrara, Annalisa Franco, and Davide Maltoni. The magic passport. In *IEEE International Joint Conference on Biometrics*, 2014. 5

[19] Matteo Ferrara, Annalisa Franco, and Davide Maltoni. Face Demorphing. *IEEE Transactions on Information Forensics and Security*, 13(4):1008–1017, 2018. 1, 5

[20] Matteo Ferrara, Annalisa Franco, and Davide Maltoni. Face demorphing in the presence of facial appearance variations. In *Proceedings of European Signal Processing Conference (EUSIPCO)*, pages 2365–2369, 2018. 1

[21] Matteo Ferrara, Annalisa Franco, Davide Maltoni, and Yunlian Sun. On the impact of alterations on face photo recognition accuracy. In *Proceedings of International Conference on Image Analysis and Processing (ICIAP)*, 2013. 1

[22] Sylvain Gugger, Lysandre Debut, Thomas Wolf, Philipp Schmid, Zachary Mueller, Sourab Mangrulkar, Marc Sun, and Benjamin Bossan. Accelerate: Training and inference at scale made simple, efficient and adaptable. <https://github.com/huggingface/accelerate>, 2022. 5

[23] Jonathan Ho, Ajay Jain, and Pieter Abbeel. Denoising Diffusion Probabilistic Models. In *Proceedings of Advances in Neural Information Processing Systems*, volume 33, pages 6840–6851, 2020. 3

[24] Elad Hoffer and Nir Ailon. Deep metric learning using triplet network. In *Proceedings of International Workshop on Similarity-Based Pattern Recognition*, 2014. 7

[25] Phillip Isola, Jun-Yan Zhu, Tinghui Zhou, and Alexei A. Efros. Image-to-image translation with conditional adversarial networks. In *Proceedings of IEEE Conference on Computer Vision and Pattern Recognition (CVPR)*, pages 5967–5976, 2017. 4

[26] Tero Karras, Miika Aittala, Janne Hellsten, Samuli Laine, Jaakko Lehtinen, and Timo Aila. Training generative adversarial networks with limited data. In *Proceedings of Advances in Neural Information Processing Systems*, 2020. 5

[27] Tero Karras, Samuli Laine, and Timo Aila. A style-based generator architecture for generative adversarial networks. In *Proceedings of IEEE/CVF Conference on Computer Vision and Pattern Recognition (CVPR)*, pages 4396–4405, 2019. 6

[28] Tero Karras, Samuli Laine, Miika Aittala, Janne Hellsten, Jaakko Lehtinen, and Timo Aila. Analyzing and Improving the Image Quality of StyleGAN. In *Proceedings of the IEEE/CVF Conference on Computer Vision and Pattern Recognition (CVPR)*, 2020. 2, 5

[29] Minchul Kim, Anil K Jain, and Xiaoming Liu. Adaface: Quality Adaptive Margin for Face Recognition. In *Proceedings of the IEEE Conference on Computer Vision and Pattern Recognition (CVPR)*, 2022. 5

[30] Davis E. King. Dlib-ml: A Machine Learning Toolkit. *The Journal of Machine Learning Research*, 10:1755–1758, Dec. 2009. 6

[31] Diederik P. Kingma and Jimmy Ba. Adam: A method for stochastic optimization. In Yoshua Bengio and Yann LeCun, editors, *3rd International Conference on Learning Representations, (ICLR)*, 2015. 5

[32] Diederik P. Kingma and Max Welling. Auto-Encoding Variational Bayes. In *Proceedings of International Conference on Learning Representations, (ICLR)*, 2014. 4

[33] Min Long, Jun Zhou, Le-Bing Zhang, Fei Peng, and Dengyong Zhang. Adff: Adaptive de-morphing factor framework

for restoring accomplice's facial image. *IET Image Processing*, 18(2):470–480, 2024. 1

[34] Satya Mallick. Face morph using opencv — c++ / python. *LearnOpenCV*, 2016. 6

[35] Mehdi Mirza. Conditional generative adversarial nets. *arXiv preprint arXiv:1411.1784*, 2014. 2

[36] Matthias Monroy. Laws against morphing. Security Architectures and the Police Collaboration in the EU, 2020. 1

[37] Tom Neubert, Andrey Makrushin, Mario Hildebrandt, Christian Kraetzer, and Jana Dittmann. Extended StirTrace Benchmarking of Biometric and Forensic Qualities of Morphed Face Images. *IET Biometrics*, 7:325–332, 2018. 5

[38] Mei Ngan, Patrick Grother, Kayee Hanaoka, and Jason Kuo. Face Recognition Vendor Test (FRVT) Part 4: MORPH - Performance of Automated Face Morph Detection. NIST Interagency/Internal Report (NISTIR), National Institute of Standards and Technology, Gaithersburg, MD, 2020-03-06 2020. 1

[39] Fei Peng, Le-Bing Zhang, and Min Long. FD-GAN: Face de-morphing generative adversarial network for restoring accomplice's facial image. *IEEE Access*, 2019. 1, 3

[40] Alyssa Quek. Face morpher. 2, 5

[41] R. Raghavendra, Kiran B. Raja, Sushma Venkatesh, and Christoph Busch. Transferable Deep-CNN Features for Detecting Digital and Print-Scanned Morphed Face Images. In *Proceedings of 2017 IEEE Conference on Computer Vision and Pattern Recognition Workshops (CVPRW)*, pages 1822–1830, 2017. 5

[42] K. Bommanna Raja, Matteo Ferrara, Annalisa Franco, Luuk J. Spreeuwers, Ilias Batskos, Florens de Wit, Marta Gomez-Barrero, Ulrich Scherhag, Daniel Fischer, Sushma Krupa Venkatesh, Jag Mohan Singh, Guoqiang Li, Loïc Bergeron, Sergey Isadskiy, Raghavendra Ramachandra, Christian Rathgeb, Dinusha Frings, Uwe Seidel, Fons Knopjes, Raymond N. J. Veldhuis, Davide Maltoni, and Christoph Busch. Morphing attack detection-database, evaluation platform, and benchmarking. *IEEE Transactions on Information Forensics and Security*, 16:4336–4351, 2020. 1

[43] K. Bommanna Raja, Matteo Ferrara, Annalisa Franco, Luuk J. Spreeuwers, Ilias Batskos, Florens de Wit, Marta Gomez-Barrero, Ulrich Scherhag, Daniel Fischer, Sushma Krupa Venkatesh, Jag Mohan Singh, Guoqiang Li, Loïc Bergeron, Sergey Isadskiy, Raghavendra Ramachandra, Christian Rathgeb, Dinusha Frings, Uwe Seidel, Fons Knopjes, Raymond N. J. Veldhuis, Davide Maltoni, and Christoph Busch. Morphing Attack Detection-Database, Evaluation Platform, and Benchmarking. *IEEE Transactions on Information Forensics and Security*, 16:4336–4351, 2020. 3

[44] Robin Rombach, Andreas Blattmann, Dominik Lorenz, Patrick Esser, and Björn Ommer. High-Resolution Image Synthesis with Latent Diffusion Models . In *Proceedings of IEEE/CVF Conference on Computer Vision and Pattern Recognition (CVPR)*, pages 10674–10685, June 2022. 2

[45] Robin Rombach, Andreas Blattmann, Dominik Lorenz, Patrick Esser, and Björn Ommer. High-resolution image synthesis with latent diffusion models. In *Proceedings of the IEEE/CVF Conference on Computer Vision and Pattern Recognition (CVPR)*, pages 10684–10695, June 2022. 4, 5

[46] Eklavya Sarkar, Pavel Korshunov, Laurent Colbois, and Sébastien Marcel. Vulnerability Analysis of Face Morphing Attacks from Landmarks and Generative Adversarial Networks. *arXiv preprint arXiv:2012.05344*, 2020. 6

[47] Mallick Satya. Face morph using opencv — c++ / python. 2016. 5

[48] Guilherme Schardong, Tiago Novello, Hallison Paz, Iurii Medvedev, Vinícius da Silva, Luiz Velho, and Nuno Gonçalves. Neural Implicit Morphing of Face Images. In *Proceedings of the IEEE/CVF Conference on Computer Vision and Pattern Recognition (CVPR)*, pages 7321–7330, June 2024. 2

[49] Ulrich Scherhag, Luca Debiasi, Christian Rathgeb, Christoph Busch, and Andreas Uhl. Detection of Face Morphing Attacks Based on PRNU Analysis. In *Proceedings of IEEE Transactions on Biometrics, Behavior, and Identity Science*, 1(4):302–317, 2019. 5

[50] Ulrich Scherhag, Christian Rathgeb, and Christoph Busch. Towards detection of morphed face images in electronic travel documents. In *Proceedings of IAPR International Workshop on Document Analysis Systems (DAS)*, pages 187–192, 2018. 1

[51] Ulrich Scherhag, Christian Rathgeb, Johannes Merkle, and Christoph Busch. Deep Face Representations for Differential Morphing Attack Detection. *IEEE Transactions on Information Forensics and Security*, 15:3625–3639, 2020. 6

[52] Nitish Shukla. SDeMorph: Towards Better Facial Demorphing from Single Morph. In *Proceedings of IEEE International Joint Conference on Biometrics (IJCB)*, 2023. 1, 2, 3, 4, 6, 8

[53] Nitish Shukla and Arun Ross. dc-GAN: Dual-Conditioned GAN for Face Demorphing From a Single Morph. *arXiv preprint arXiv:2411.14494*, 2024. 2

[54] Nitish Shukla and Arun Ross. Facial Demorphing via Identity Preserving Image Decomposition. In *Proceedings of IEEE International Joint Conference on Biometrics (IJCB)*, 2024. 1, 2, 3, 4, 6, 8

[55] Nitish Shukla and Arun Ross. Metric for evaluating performance of reference-free demorphing methods. In *Proceedings of IEEE/CVF Winter Conference on Applications of Computer Vision Workshops (WACVW)*, 2025. 5, 6

[56] Dmitry Ulyanov, Andrea Vedaldi, and Victor S. Lempitsky. Instance normalization: The missing ingredient for fast stylization. *ArXiv*, abs/1607.08022, 2016. 5

[57] Von Raphael Thelen und Judith Horchert. <https://www.spiegel.de/netzwelt/netzpolitik/biometrie-im-reisepass-peng-kollektiv-schmuggelt-fotomontage-in-ausweis-a-1229418.html>, 2018. 1

[58] Yuxin Wu and Kaiming He. Group normalization. In *Computer Vision – ECCV 2018: 15th European Conference, Munich, Germany, September 8–14, 2018, Proceedings, Part XIII*, page 3–19, Berlin, Heidelberg, 2018. Springer-Verlag. 5

[59] Haoyu Zhang, Sushma Venkatesh, Raghavendra Ramachandra, Kiran Raja, Naser Damer, and Christoph Busch. MIP-GAN—generating strong and high quality morphing attacks

using identity prior driven gan. *IEEE Transactions on Biometrics, Behavior, and Identity Science*, 3(3), 2021. 2

[60] K. Zhang, Z. Zhang, Z. Li, and Y. Qiao. Joint Face Detection and Alignment Using Multitask Cascaded Convolutional Networks. *IEEE Signal Processing Letters*, 23(10):1499–1503, 2016. 6

[61] Xuaner Zhang, Ren Ng, and Qifeng Chen. Single Image Reflection Separation with Perceptual Losses . In *Proceedings of IEEE/CVF Conference on Computer Vision and Pattern Recognition (CVPR)*, pages 4786–4794, June 2018. 7

[62] Zhengxia Zou, Sen Lei, Tianyang Shi, Zhenwei Shi, and Jieping Ye. Deep Adversarial Decomposition: A Unified Framework for Separating Superimposed Images . In *Proceedings of IEEE/CVF Conference on Computer Vision and Pattern Recognition (CVPR)*, pages 12803–12813, 2020. 3, 4, 7